5-12-2018

3-D Seismic Investigation of a Gas Hydrate and Fluid Flow System on an Active Mid-Ocean Ridge; Svyatogor Ridge, Fram Strait

Kate A. Waghorn
The Arctic University of Norway

Stefan Bunz
The Arctic University of Norway

Andreia Plaza-Faverola
The Arctic University of Norway

Joel E. Johnson
University of New Hampshire, Durham, joel.johnson@unh.edu

Recommended Citation
Waghorn, K.A., Bünz, S., Plaza-Faverola, A., and Johnson, J.E., 2018. 3-D Seismic Investigation of a Gas Hydrate and Fluid Flow System on an Active Mid-Ocean Ridge; Svyatogor Ridge, Fram Strait. Geochemistry, Geophysics, Geosystems, 19. https://doi.org/10.1029/2018GC007482.

AGU100 ADVANCING EARTH AND SPACE SCIENCE

Geochemistry, Geophysics, Geosystems

RESEARCH ARTICLE
10.1029/2018GC007482

Key Points:
- A gas hydrate system is imaged with 3-D seismic data south of Vestnesa Ridge and exists on young, warm crust near the plate boundary
- The system is seeping fluid at the seafloor episodically, likely controlled by seismic activity
- We identify fracture networks, which we suggest a proxy to identify the extent of gas hydrate within the sediment column

Correspondence to:
K. A. Waghorn,
kate.a.waghorn@uit.no

Citation:
Waghorn, K. A., Bünz, S., Plaza-Faverola, A., & Johnson, J. E. (2018). 3-D seismic investigation of a gas hydrate and fluid flow system on an active mid-ocean ridge; Svyatogor Ridge, Fram Strait. *Geochemistry, Geophysics, Geosystems*, *19*, 2325–2341. https://doi. org/10.1029/2018GC007482

Received 15 FEB 2018
Accepted 8 MAY 2018
Accepted article online 12 MAY 2018
Published online 8 AUG 2018

3-D Seismic Investigation of a Gas Hydrate and Fluid Flow System on an Active Mid-Ocean Ridge; Svyatogor Ridge, Fram Strait

Kate A. Waghorn[1], Stefan Bünz[1], Andreia Plaza-Faverola[1], and Joel E. Johnson[2]

[1]Department of Geosciences, Centre for Arctic Gas Hydrate, Environment and Climate, UiT—The Arctic University of Norway, Tromsø, Norway, [2]Department of Earth Sciences, University of New Hampshire, Durham, NH, USA

Abstract Tectonic settings play a large role in the development of fluid flow pathways for gas migrating through sedimentary strata. Gas hydrate systems worldwide are located on either the slopes of passive continental margins, often in large contourite deposits, or in accretionary wedges on subduction margins. The Svyatogor Ridge, however, located at the northwestern flank of the Knipovich Ridge and south of the Molloy Transform Fault (Fram Strait), is a gas hydrate system which is located on an actively spreading margin. Svyatogor Ridge has evidence of shallow gas accumulations; a strong BSR indicating a gas hydrate and underlying free gas system, and fluid flow pathways to the seafloor culminating in pockmarks. Using a high-resolution P-Cable 3-D seismic survey, we investigate how tectonic and sedimentary regimes have influenced the formation of this well-developed gas hydrate system. Large-scale basement faults identified in the seismic data are interpreted as detachment faults, which have exhumed relatively young ultramafic rocks. These detachment faults act as conduits for fluid flow, and are responsible for the formation of folds in the overlying sediments that are breached by faults. We propose a model for fluid flow within this system whereby as sedimentary faults breach upward through the sedimentary strata, fluid is able to migrate further upward. We find that the tectonic regime on Svyatogor Ridge is the dominant driver of fluid migration and episodic release at the seafloor.

1. Introduction

Gas hydrates are solid compounds of water and gas (i.e., dominantly methane), which are stable in marine sediments or permafrost regions at high pressures and low temperatures (i.e., Sloan, 1998). Determinants for gas hydrate formation are salinity (high salinity inhibits hydrate formation), porosity, and a sufficient gas input. The gas that sustains gas hydrate accumulations in shallow sediments has been found to be predominantly of microbial or thermogenic origin (Klauda & Sandler, 2005). In the case of microbial in situ methane production, an input of organic matter into the system is also necessary (Paull et al., 1994). Therefore, many of the subaqueous gas hydrate and related fluid flow system occurrences worldwide are observed on TOC-rich sedimented continental margins (i.e., Hikurangi Margin (Pecher et al., 2005), Cascadia Margin (Suess et al., 1999), Gulf of Mexico (Shipley et al., 1979)) or in large contourite deposits (i.e., Vestnesa Ridge (Bünz et al., 2012), Blake Ridge (Faugères et al., 1999)) as these settings generally meet all the conditions for both gas hydrate formation and stability. Distal settings (i.e., abyssal plains), on the other hand, are generally characterized by deposition of clays and silts, and lower organic matter fluxes to the seafloor (Klauda & Sandler, 2005; Müller & Suess, 1979) and the common assumption is that these are not ideal settings for gas hydrate formation, even though they may fall within the gas hydrate stability zone.

In the Fram Strait, the Western Svalbard Margin and Vestnesa Ridge are known for storing large quantities of methane within the sedimentary strata, where large amounts of this shallow gas is sequestrated as gas hydrate (Bünz et al., 2012; Hustoft et al., 2009; Vanneste et al., 2005). The Western Svalbard margin is a passive continental margin that evolved in connection with the onset of rifting in the North Atlantic (e.g., Engen et al., 2008; Lundin & Doré, 2002). Vestnesa Ridge formed as a large contourite deposit that extends off the continental margin crossing the continental-oceanic crust transition (Bünz et al., 2012; Eagles et al., 2015; Engen et al., 2008). Although the distribution of fluid flow related features developed through the gas hydrate zone on Vestnesa Ridge is correlated with the presence of faults (Plaza-Faverola et al., 2015), the

gas hydrate system here is assumed to have developed post-rift (Bünz et al., 2012; Eiken & Hinz, 1993; Engen et al., 2008). However, to the west of the Western Svalbard Margin and south of Vestnesa Ridge is the Knipovich Ridge, which is an ultraslow spreading ridge (Dick et al., 2003). In such ultraslow settings, magmatism is limited and low-angle detachment faults accommodate the majority plate motion and can remain active for 1–3 Myr (Escartin et al., 2008; Tucholke et al., 1998). The Arctic mid-ocean ridges are all ultraslow and in particular, low-angle detachment faults and exhumed serpentinized peridotites have been observed and/or sampled on the Gakkel Ridge, Lena Trough, and Molloy Ridge (Dick et al., 2003; Michael et al., 2003; Snow et al., 2001). Abiotic methane has been, in recent years, identified as another potential gas source available for gas hydrate formation in slow to ultraslow spreading environments (Johnson et al., 2015; Rajan et al., 2012), forming during serpentinization of ultramafic rocks (Etiope & Sherwood Lollar, 2013). Serpentinites sampled on the seafloor in slow and ultraslow spreading mid-ocean ridges are often found in close proximity to detachment faults (Cann et al., 1997; Kelley et al., 2005), which provide easy access for seawater to drive serpentinization reactions. Due to the limited life span of slip on a detachment fault and the temperature range for maximum serpentinization, the window to form serpentinized methane is limited to young crust close to the spreading axis (Johnson et al., 2015). Additionally, serpentinites are commonly observed at the junctures between spreading ridges and transform faults, where detachment faults are well developed (Tucholke et al., 1998).

Due to the proximity of the Arctic mid-ocean ridges to the Western Svalbard Margin, and their ultraslow spreading rates, the Arctic mid-ocean ridges are often sedimented, and magma-limited conditions create geothermal gradients lower than at intermediate to fast spreading ridges. The flanks of the Knipovich Ridge and Molloy Ridge are not only within the temperature and pressure regime required for gas hydrate stability, but also are characterized by having similar sedimentary depositional regimes (Eiken & Hinz, 1993) and potentially even their own methane source—serpentinized abiotic methane (Johnson et al., 2015; Rajan et al., 2012).

Svyatogor Ridge is a sedimented, elongated ridge located on the flank of the Knipovich Ridge at the inner junction with the Molloy Transform Fault. Previous work has documented the presence of a gas hydrate system on the Svyatogor Ridge (Johnson et al., 2015). Unlike the other Fram Strait gas hydrate reservoirs, the gas hydrate system on the Svyatogor Ridge is on the flank of an actively spreading mid-ocean ridge, implying that unlike the other Arctic gas hydrate systems, Svyatogor Ridge is in an actively rifting environment. Using high-resolution 3-D seismic data, we investigate the first gas hydrate system identified on the flank of an actively rifting ultraslow spreading margin. Based on detailed descriptions of tectonic and sedimentary structures characterizing the gas hydrate bearing ridge, we explore the implications that this tectonically active ultraslow spreading setting has on the development of a gas hydrate system and associated seafloor seepage system.

2. Geologic Setting and Tectonic History

2.1. Study Area

Svyatogor Ridge is a contourite driven sedimented ridge with a length of 46 km and a width of ~5 km (Figure 1) (Johnson et al., 2015). Our study focuses on the southernmost part of the ridge.

2.2. Tectonic Background

The ultraslow spreading Knipovich Ridge extends for ~550 km in N-S direction (Okino et al., 2002), with a half-spreading rate for the Knipovich Ridge of 6.2 mm/yr, on the western, faster moving, side of the Ridge (Ehlers & Jokat, 2009). The Knipovich Ridge connects the Gakkel Ridge in the Arctic Ocean to the Mohns Ridge through a number of transform faults and small spreading centers (Figure 1). The Gakkel and Mohns Ridges most likely began spreading during Chron 24 at 53 Ma (Ehlers & Jokat, 2009; Vogt et al., 1978), and the Knipovich Ridge began propagating northward at Chron 13, 33 Ma (Ehlers & Jokat, 2009; Talwani & Eldholm, 1977). At the northernmost segment of Knipovich Ridge, magnetic anomaly C6 (19.6 Ma) is clearly delineated, and C5 (9.8 Ma) is present as a weaker lineation (Engen et al., 2008) on the western side of the Ridge. Conjugate magnetic anomalies are not present on the Svalbard side of the Ridge, leading Engen et al. (2008) to suggest that the junction between the Molloy Transform Fault and Knipovich Ridge has migrated northward. Faults and rift escarpments further north suggest that the Knipovich ridge is continuing to propagate northward under the West Svalbard Margin (Crane et al., 2001). Due to the nature of the

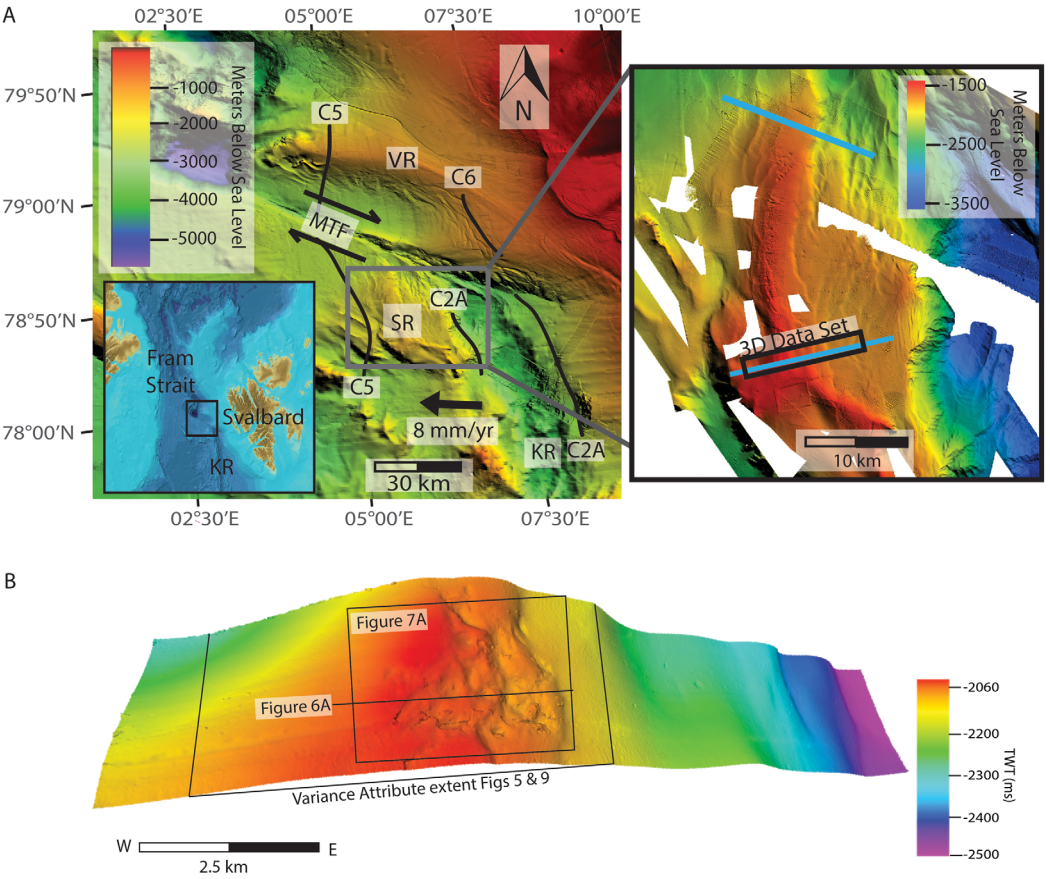

Figure 1. (a) The Svyatogor Ridge is a 46 km long, ~5 km wide feature at the intersection between the Molloy Transform Fault (MTF) and the Knipovich Ridge (KR). The Knipovich Ridge has a spreading rate of ~8 mm/yr (Ehlers & Jokat, 2009). Svyatogor Ridge is located between Chrons 5 and 2A (C2A, C5), correlating to 9.8 and 2.8 Ma, respectively (Engen et al., 2008). The location of the 3-D P-Cable Seismic survey is marked by the black box in the inset and seismic examples from Johnson et al. (2015) are marked by blue lines. Other tectonic and geologic features in the Fram Strait are the Vestnesa Ridge (VR), Molloy Ridge (MR), Yermak Plateau (YP), Lena Trough (LT), and Gakkel Ridge (GR). (b) Position of Figures 5–7 and 9 in relation to the 3-D seismic cube.

geologic and tectonic setting of the study area, close to the Knipovich Ridge, the crust is young and close to the seafloor (Amundsen et al., 2011).

2.3. Seismic Stratigraphy

Three main stratigraphic units provide chronological constraints on the West Svalbard Margin (Eiken & Hinz, 1993). YP-1 is the oldest unit, composed of syn-rift and post-rift sediments, which deposited directly on oceanic crust; YP-2 sequence comprises the onset of contourite facies with a basal age between 11 and 14.6 Ma; and YP-3 corresponds to the onset of glacially transported sediments, where contourites and glaciomarine turbidites and debris flows are the predominant facies. Correlation to cores drilled during Ocean Drilling Program Leg 151 (Geissler et al., 2011) provides the age control for these seismic stratigraphic units. The boundary between YP-2 and YP-3 is estimated to be 2.7 Ma (Eiken & Hinz, 1993; Mattingsdal et al., 2014), and has been identified in the region comprising the Yermak Plateau, the Vestnesa Ridge, and offshore Prins Karls Forland (Eiken & Hinz, 1993; Hustoft et al., 2009; Mattingsdal et al., 2014). Based on the supposition that the Svyatogor Ridge was offset to the west during growth of Vestnesa Ridge across the MTF during the last 2–3 Ma (Johnson et al., 2015), YP-2 and YP-3 seismic stratigraphic units should also be present on the Svyatogor Ridge. YP-1, however, is most likely too old compared to the estimated crustal age to be present on Svyatogor Ridge (Engen et al., 2008; Mattingsdal et al., 2014).

2.4. Oceanography

The Fram Strait channels warm, saline waters from the North Atlantic into the Arctic Ocean, and transports cold Arctic water southward (Beszczynska-Möller et al., 2012). The West Spitsbergen Current brings North Atlantic water northward, and is an important sediment supply system for the Western Svalbard Margin, having deposited the muddy-silty contourite deposits that dominate sedimentation (Howe et al., 2008; Rebesco et al., 2013). Although paleo-current indications suggest the West Spitsbergen Current has migrated up the West Svalbard Margin slope over time (Eiken & Hinz, 1993), this current may have been influencing the Svyatogor Ridge in the past (Johnson et al., 2015), thus, driving sedimentation that ultimately hosts the gas hydrate and free gas system observed there today. As the West Spitsbergen Current has migrated upslope through time, we expect the WSC influenced sedimentation to decrease through time on Svyatogor Ridge.

3. Data and Methods

A 2 $\times$ 10 km high-resolution P-Cable 3-D seismic data set was acquired in 2014 aboard R/V Helmer Hanssen. P-Cable seismic data were recorded using 14, 25 m long streamers spaced 12.5 m apart with eight channels per streamer (e.g., Planke et al., 2009). The source used was a mini-GI air gun with a capacity of 15/15 $in.^3$, fired every 5 s with the ship maintaining a speed of 4 km and sailing line spacing of $\sim$60 m. Data processing steps included: insertion of navigation data, CDP-Binning at 6.25 $\times$ 6.25 m (fold of approximately 7 traces per CDP bin), static corrections, bandpass filtering with a frequency of 10–20–400–500 Hz, attenuation and spherical divergence correction, NMO correction, stacking, interpolation in crossline direction and a 3-D Stolt (post-stack)|Migration. We used a constant velocity of 1,600 m/s for migration, constrained for the imaged sedimentary infill by Ritzmann et al. (2004), who used Ocean Bottom Seismometers for velocity analysis. Dominant frequency of this data is 120 Hz, so the vertical data resolution is $<$3.2 m (λ/4) at the seafloor assuming a water velocity of 1,490 m/s (measured by CTD at beginning of surveying). Data penetration is restricted to 3,200 ms TWT. Seismic interpretation used commercially available seismic interpretation software (Petrel). Variance maps were generated along major reflections for fault analysis and depositional reconstruction carried out for constraining the evolution of the study area. Seismic results are analyzed together with bathymetry data with a resolution of $\sim$10–20 m collected aboard the R/V Helmer Hanssen between 2014 and 2016. Repeated water column acoustic mapping (June 2014 and October 2015) during CAGE cruises 14-1, 14-2, and 15-6 reveled no active fluid expulsion above pockmarks on the crest of Svyatogor Ridge.

4. Results and Interpretations

4.1. Distinct Depositional Periods

Four main depositional periods (S1–S4) are identified in addition to the acoustic basement, based on: (1) the seismic character of the reflections; (2) faulting pattern; and time framework (i.e., syn-rift or post-rift deposition) (Figure 2).

Johnson et al. (2015) define the basement in this study area, which are indicated by the transition in seismic response between sediments and oceanic basement. Using the nearest published seafloor sampling results, seismic refraction data, and the tectonic setting, Johnson et al. (2015) suggest that the basement in the study area is likely composed of serpentinized ultramafic rocks. The basement has two prominent highs (East Peak, West Peak; Figure 3a), with a depression located in between. Associated with these two peaks, the acoustic basement tilts creating an additional two small basins at the western and eastern ends of the data set (Figure 3). Within the unit defined as basement, there are no seismic indications of stratified reflections from sediments. We interpret the basement as young crust formed as part of the Knipovich Ridge spreading regime.

Pockets of sediments infilling acoustic basement lows (Figures 2 and 3a) characterize the first period of deposition (Unit S4). In the central depression between the two basement peaks, this unit appears to onlap against the East Peak but abruptly truncates against the West Peak. Amplitude of reflections in this unit is very low. All reflectors in this unit dip at similar angles to the acoustic basement (Figure 3a). The reflector marking the top of Unit S4 appears to be erosional (truncating lower reflectors) on the western side of West

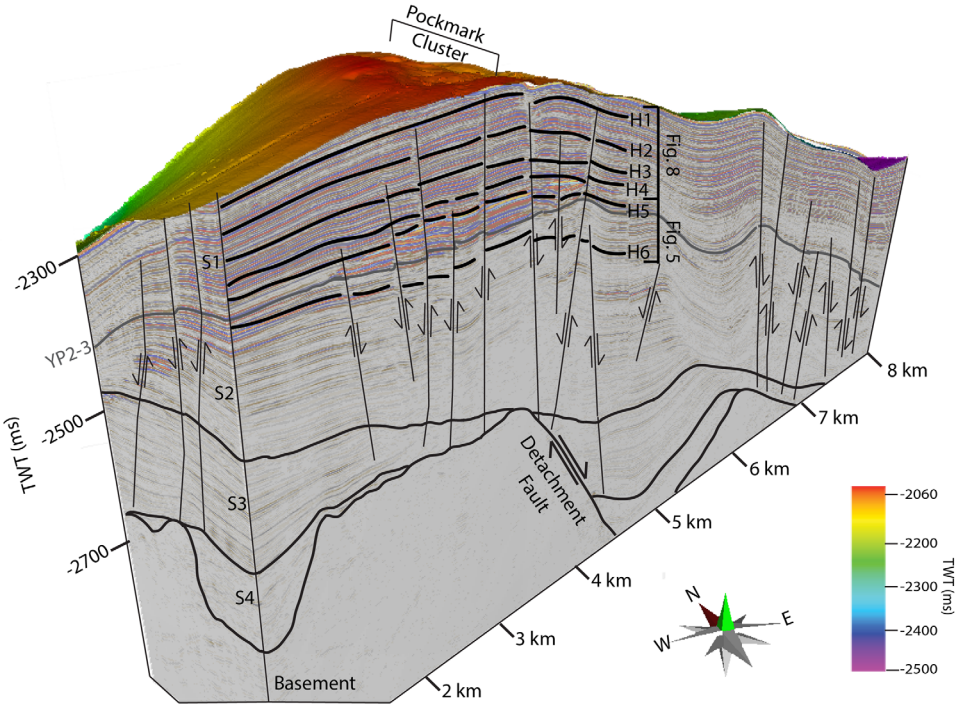

Figure 2. The data set is divided into four units representing depositional periods (S4–S1) and basement. These depositional periods are defined based on seismic properties that indicated a change in depositional regime and rock/sediment properties. Locations of structural maps in Figures 5 and 8 are annotated on this section. WP and EP are the west and east basement peaks, respectively.

Peak. Unit S4 is interpreted to be sedimentation infilling the basement highs and lows. It is difficult to interpret further owing to the extremely low amplitudes. The rotation of the few reflectors we could identify suggests this unit has tilted because of tectonic event(s).

Unit S3 also infills basement lows; however, it is not localized in the same manner as S4; the top reflections of this unit are nearly continuous throughout the entire data set, except in one area (west peak) where the acoustic basement protrudes above this unit (Figures 2 and 3a). While in the west of the data set, reflectors are subhorizontal to slightly rotated, the eastern half of this unit is rotated to conform to the dip trend of the acoustic basement (Figures 2 and 3a). Overall, the amplitudes and reflection frequency of this unit are low; however, moving upward through this unit reflectors appears to become increasingly less rotated (Figure 3a). We therefore interpret this unit to have continued to infill basement lows after the deposition of Unit S4.

Depositional period S2 consists of mostly subhorizontal deposition in the west and dipping reflectors in the east. In this unit, there is thickening of sedimentary packages toward the east (Figure 3). Disruption and vertical offset of reflections are prevalent within Unit S2. Based on the correlation with regional seismic lines (e.g., Hustoft et al., 2009), we interpret that the top reflection of our S2 depositional period coincides with the YP2/YP3 boundary. This indicates that the sediment deposited in this unit is older than 2.7 Ma. In addition, the unit thickens eastward so this unit is interpreted to deposit as the WSC was moving east, while simultaneously the Knipovich Ridge was propagating Svyatogor Ridge westward.

Depositional period S1 is composed of mostly subhorizontal reflectors in the west and dipping reflectors in the east (Figure 3). Unit S1 shows a clear thickening trend of sedimentary packages toward the east (Figure 3b). The amplitudes in this depositional period also cycle from high amplitude to low amplitude; however, the transition to low amplitude is abrupt and therefore there is a predominance of high amplitude (Figure 3a). Frequency of reflections in this unit is high. Like Unit S2, disruption and vertical offset of reflections are common. The uppermost reflector in this unit is the seafloor and the base has been correlated as YP2/3 (e.g., Hustoft et al., 2009); therefore, this unit must correlate to YP3 ($<$2.7 Ma) sediment. The eastward thickening of this unit is interpreted to result from the combined effects of the eastward migration of the WSC and the westward offset of the ridge along the MTF.

10.1029/2018GC007482

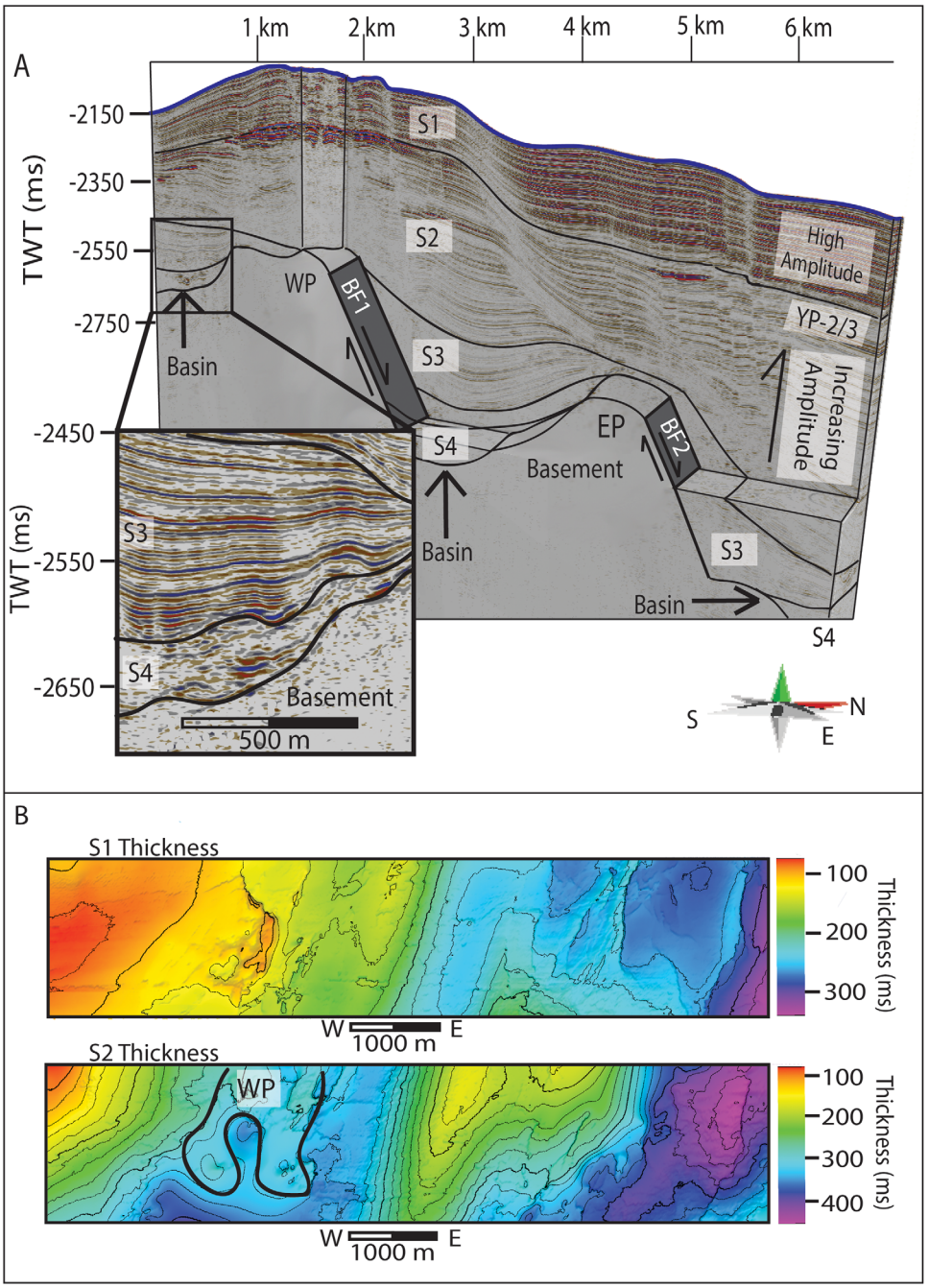

Figure 3. (a) The acoustic basement has two main peaks (WP, West Peak; EP, East Peak) that are defined by two normal faults, with basins surrounding the peaks. Units S4 and S3 infill these basement highs. Units S2 and S1 are composed of mainly subhorizontal reflectors in the west and dipping reflectors in the east. Inset: Units S4 and S3 are slightly rotated, and stretched, to conform to the tilt of the basement. This has led to the interpretation that these units have been deposited while these faults were active. (b) Isopach maps of Units S1 and S2 show that eastward thickening of strata is most pronounced in S2. Section marked "WP" is where the basement peak West Peak outcrops into S2.

4.2. Fault Analysis

4.2.1. Major Tectonic Faults

Two normal faults (BF1, BF2) were identified at the lower limit of penetration of the data set (Figure 4). These faults occur in the acoustic basement and do not extend upward into the sedimentary sequences (Figure 4). The western-most basement fault (BF1) is the best imaged and closer to the surface. The eastern-

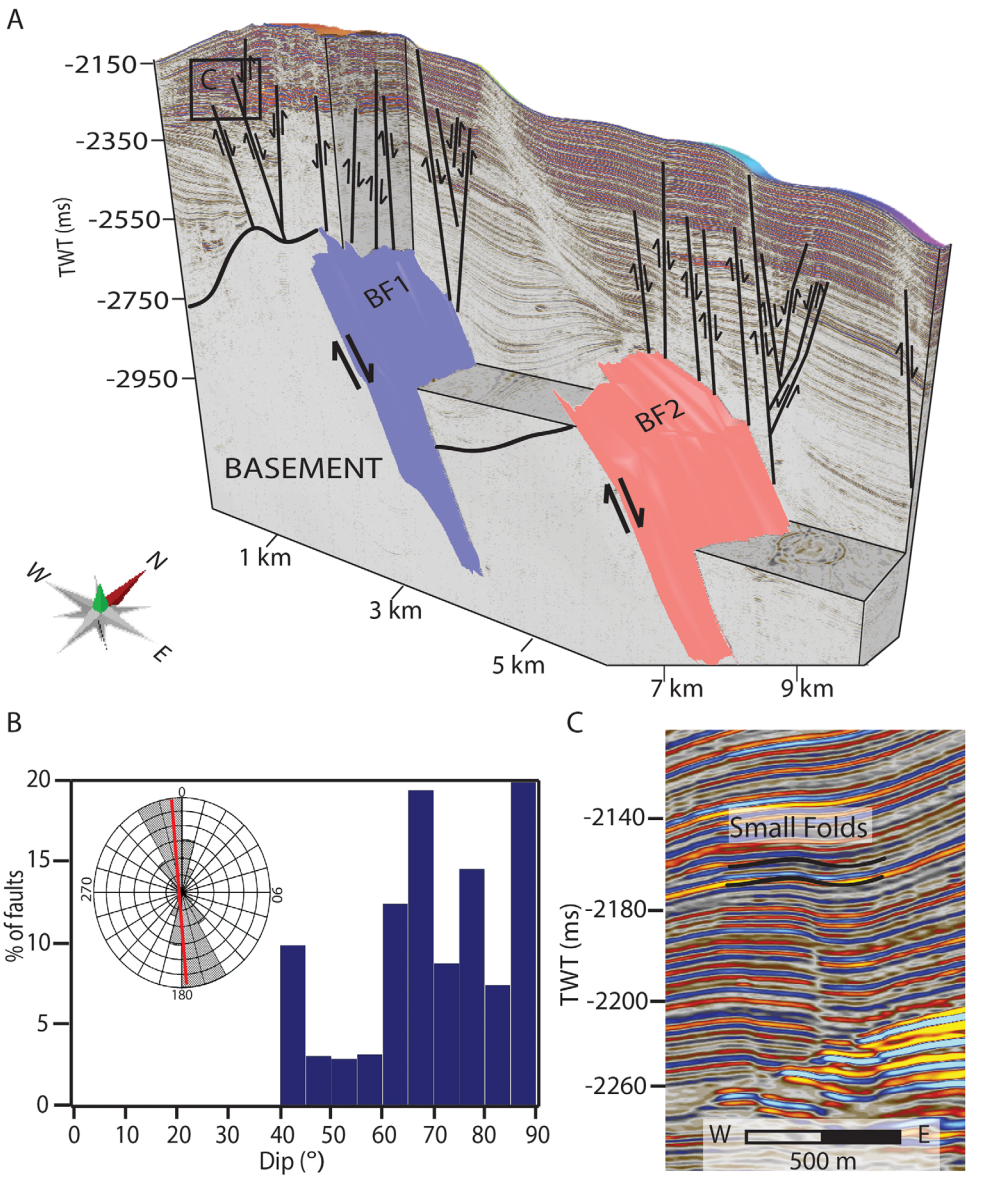

Figure 4. (a) BF1 and BF2 are two large normal detachment faults identified within the data set. These faults do not extend beyond the basement however, sedimentary fault arrays occur exclusively around the area where the basement faults occur. (b) The sedimentary faults mostly conform to the regional tectonic regime (strike of Knipovich Ridge marked in red on Stereonet, from Peive and Chamov (2008)). Dip of the sedimentary faults is between 40° and 90°. (c) Sedimentary faults from the eastern-most group shown in Figure 4a showing instances of small folds occurring above the fault termination, indicating that these are developing as growth faults.

most basement fault (BF2) is at the very edge of both lateral and vertical data extent; however, it is still possible to interpret a fault plane. The dip of BF1 and BF2 is calculated to be 30° and 20°, respectively (based on a velocity of 1,600 m/s adjacent to sedimentary sections), and dip azimuth of BF1 is ~80° while BF2 ~95°. Both faults conform to the regional tectonic setting. Offset of BF1 is at least 1,200 m and the offset of BF2 at least 1,000 m (Amundsen et al., 2011). These faults are interpreted to be detachment faults, which are related to spreading on the Knipovich Ridge (Amundsen et al., 2011; Johnson et al., 2015).

4.2.2. Sedimentary Faults

In the sedimentary strata, there are numerous steeply dipping normal faults present throughout the data set. These faults are NNW-SSE oriented and have dips of between 40° and 90°, although most faults dip between 60° and 90° (Figure 4). Most of the faults upwardly terminate in Unit S2 although a few terminates within Unit S1 or reach the seafloor. These faults are all concentrated around the two major tectonic faults,

BF1 and BF2, in the acoustic basement (Figure 4). These faults mostly comply with the regional tectonic setting although some at the apex of the ridge do not (Figure 4) (Peive & Chamov, 2008). Sedimentary faults nearly exclusively terminate against the basement. At the upward termination of the faults, there is often a very small fold, which is indicative of a fault propagation folding (Hardy & McClay, 1999; Jackson et al., 2006). We interpret folding at the upper terminus of sedimentary faults to indicate upward and lateral propagation of normal faults through ductile sediment deposited over more rigid basement material (e.g., Corfield & Sharp, 2000).

4.2.3. Radial Faults and Fracture Networks

Structural maps reveal smaller scale faults forming at random azimuths between larger scale NW-SE trending faults (Figure 5). We only identify this type of faulting in the area above West Peak. This type of faulting occurs in a linear, step-like fashion around a zone of acoustic blanking coincident above West Peak (Figure 5). This type of faulting is interpreted as radial faulting, and similarly to the radial-type faulting around sediment remobilization features (e.g., Hansen et al., 2005), is interpreted to be a function of the sediment doming around the peaks associated with the two major detachment faults BF1 and BF2 (Figure 4a). In this case, we interpret the structure causing sediment doming to be uplift of West Peak into the sedimentary sequence. Lastly, we also identify even smaller scale features in variance attribute that are also forming at random azimuths, and sometimes as circular features, and are often barely recognizable in the seismic section (Figure 5). These features are mostly associated with a very small depression at the upward termination, which may be interpreted as fluid flow features (Hartwig et al., 2012). As the depression structure is at the limit of seismic resolution, it is difficult to interpret whether it is a paleo-pockmark or associated with syn-tectonic infill; however, the circular features often form at intersections of the small scale, random azimuth features. Therefore, we interpret the random azimuth features as fracture networks.

4.3. Fluid Flow and Associated Gas Hydrate System

In Unit S1, located 150 ms TWT beneath the seafloor, at the apex of Svyatogor Ridge is a persistent crosscutting reflector with anomalously high amplitude, reverse polarity cf. the seafloor that simulates the seafloor

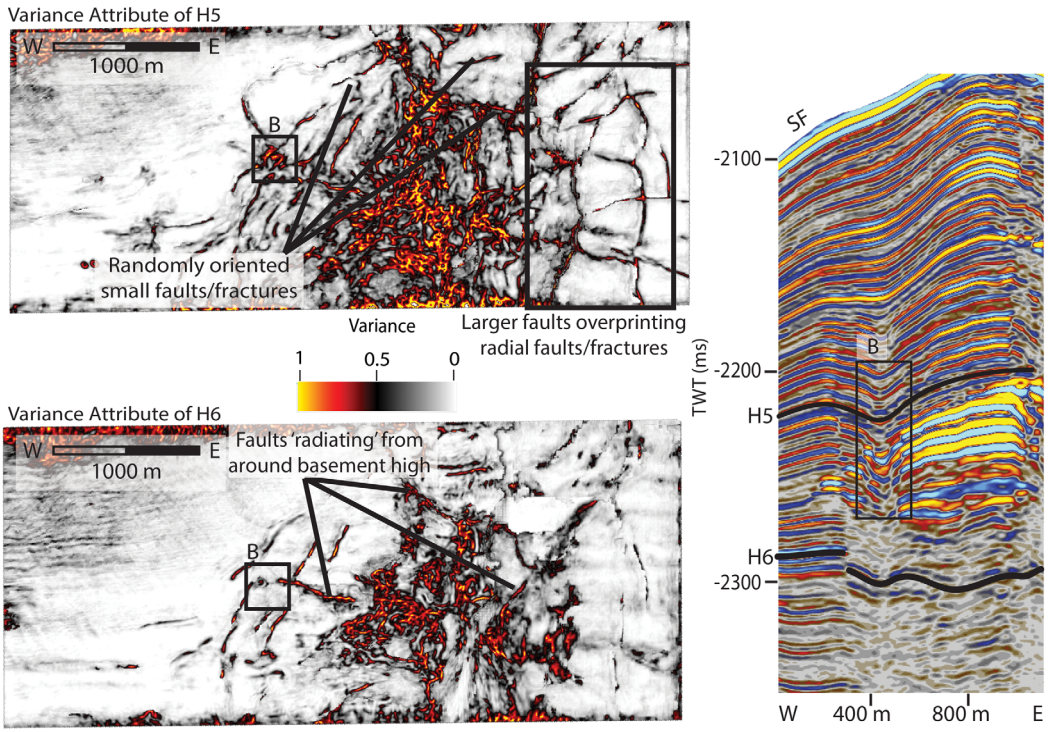

Figure 5. Structural maps (variance attribute) of horizons show radial faulting at depths greater than 2,150 ms TWT. These are interpreted to be caused by the uplift of the basement West Peak into its current position. We also identified fracture networks (b) which often present as small circular features in variance attribute, however, are often difficult to observe as faults in the seismic section. Location of horizons shown in Figure 2 and inset.

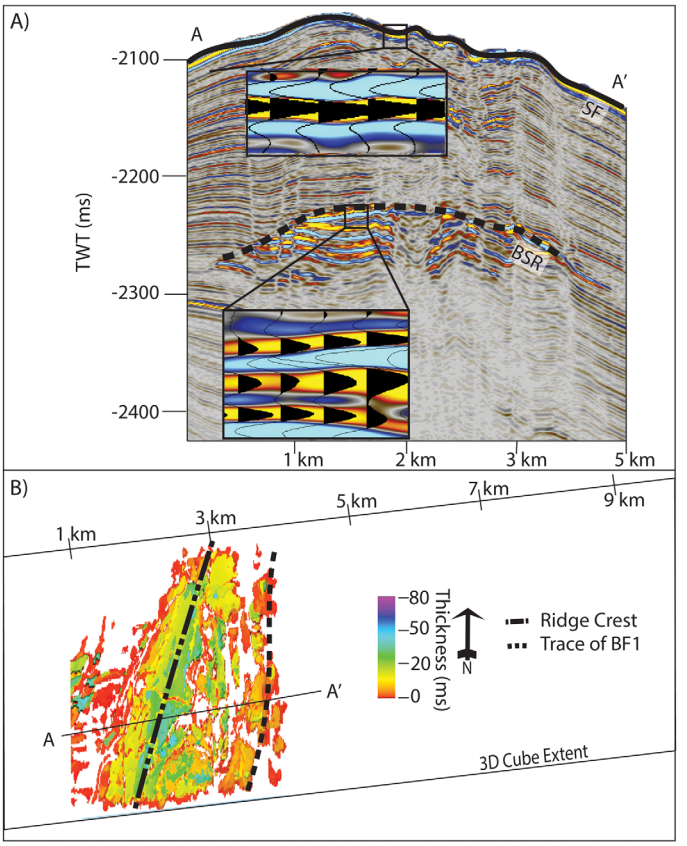

Figure 6. (a) The reflection identified as a BSR is characterized by being reverse polarity and mimicking the seafloor as well as being notably higher in amplitude than the surrounding strata. (b) The free gas zone beneath the BSR is relatively small in comparison to the extent of our 3-D cube, however important to note that it is limited to the area west of the BF1 footwall and is thickest at the ridge crest axis.

(Figure 6a). Such a distinct crosscutting reflection is known as the bottom-simulating reflector (BSR) which indicates the base of the GHSZ (Shipley et al., 1979). There is a zone (40–60 ms TWT thick) immediately below the BSR with enhanced amplitudes compared to the surrounding strata (Figure 7b).

This high amplitude zone is also a typical element of a gas hydrate system, where free gas is trapped underneath gas hydrate bearing sediments (e.g., Holbrook et al., 1996). The free gas zone in Svyatogor ridge is contained to the west of the BF1 footwall (Figure 6b), becoming thinner toward the flanks of the sedimentary ridge until disappearing ∼1 km away from the axis of the ridge (Figure 6b). Beneath the enhanced reflection zone is a diminished amplitude zone extending through Units 2, 3, and 4 (Figure 7b). This zone characterized by amplitude blanking is the result of energy attenuation and scattering when the waves travel through gas-bearing sediments (Anderson & Hampton, 1980; Cartwright & Santamarina, 2015; Løseth et al., 2009).

A number of circular-elliptical depression structures (90–350 m diameter) disturb the seafloor at the apex of Svyatogor Ridge (Figure 7a). We interpret these features as pockmarks related to fluid expulsion at the seafloor. There are two distinct fluid migration pathways leading to these seafloor pockmarks. First, underlying the apex of the ridge (Figure 7b) is a zone of hummocky, nonconformant reflections, which are notably lower in amplitude than the rest of Unit S1 (section 4.1.5). This zone is interpreted to be a zone of focused fluid migration, referred to as a chimney zone here. The second fluid migration pathway are faults that upwardly terminate at the base of pockmarks. Spatially, pockmarks with a chimney beneath occur at the crest of the ridge while pockmarks underlain by a fault occur <100 m east of the ridge crest (Figures 7a and 7b).

Within the chimney cluster, interleaved between sections of low amplitude, hummocky reflections are four horizons that have higher amplitude, are semicontinuous, and appear undulating in 2-D. In 3-D, these undulations are circular depressions, the flanks of which are truncating reflectors beneath (Figure 8). These depression structures are infilled with a low amplitude material which onlaps against the flanks of the depression (Figure 8). We interpret these features as buried pockmarks, with the disturbed, low amplitude zones beneath being individual chimneys. Buried pockmarks occur only in the chimney cluster. Although reflections are highly disturbed in the chimney cluster, we are unable to discern any faults leading to buried pockmarks. Buried pockmarks occur specifically on four stratigraphic intervals (Figure 9); however, they are not vertically stacked, nor are they of consistent size, either within the same stratigraphic interval or vertically throughout the data set; therefore, they are not velocity artifacts. Due to their locations on four specific stratigraphic intervals, these are interpreted to be recording episodic fluid expulsion at paleo-seafloors.

5. Discussion

5.1. Structural and Stratigraphic Evolution of Svyatogor Ridge

The Svyatogor Ridge has undergone much deformation as indicated by the numerous faults present in the data set. The configuration of reflections within the individual units provides information on the style and possible timing of faulting and deformation on the Svyatogor Ridge. The rotation angles and onlap/termination patterns of Units S4 and S3 indicate that these packages have undergone rotation during phases of movement on BF1 and BF2 (Figure 3). Units S2 and S1 are highly faulted, especially around the basement highs (Figures 2 and 5). This is indicative that there was still movement on the basement faults during or after deposition of these units. As the West Spitsbergen Current is the dominant sediment supply current to

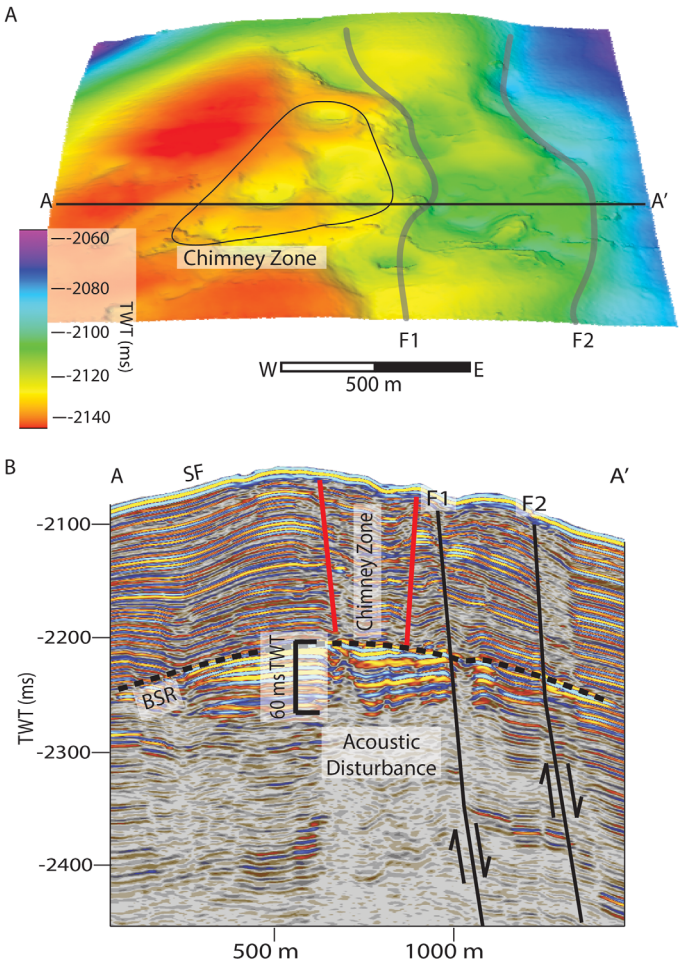

Figure 7. (a) Seafloor map (interpreted from the 3-D seismic) shows two groups of pockmarks are observed, those above the chimney zone, and those which are underlain by the western-most sedimentary fault (F1). (b) The chimney zone is immediately adjacent to F1. It is delineated by a change between regular subhorizontal deposition to hummocky irregular deposition. The free gas zone is 60 ms TWT thickest at the thickest point.

the West Svalbard Margin and Yermak Plateau (Eiken & Hinz, 1993), and that Svyatogor Ridge is isolated from downslope processes by the Knipovich Ridge axial valley, the West Spitsbergen Current has likely dominated sediment supply to Svyatogor Ridge in the past. Given that the West Spitsbergen Current has migrated upslope, away from the Svyatogor Ridge (Eiken & Hinz, 1993; Johnson et al., 2015), the Svyatogor Ridge has likely been sediment-limited since spreading began on the northern Knipovich Ridge (Johnson et al., 2015).

Two styles of faulting present in the data can be attributed to regional tectonism—the detachment faults, which are directly linked to spreading on the Knipovich Ridge (Amundsen et al., 2011; Johnson et al., 2015), and the sedimentary faults, which based on the strike of these faults, conform to the regional tectonic setting (Crane et al., 2001). There are two main possible mechanisms for the formation of such faults in this environment.

First, the creation of accommodation space as the Knipovich Ridge spreads can result in gravity driven extension (Bodego & Agirrezabala, 2013; Peel, 2014). Second, growth faulting, which occurs when a mechanically weaker material (sediment) overlies a mechanically stronger material (basement), and the stronger material faults (Hardy & McClay, 1999; Tvedt et al., 2013). As a fault in the basement moves, the sediment overlying the basement accommodates this by folding (Figure 10); however, as offset on the basement fault increases, the folds may become breached, forming the sedimentary faults (Ferrill et al., 2012; Hardy & McClay, 1999). The process of sedimentary fault propagation through this mechanism will occur at a rate determined by the movement of the basement fault (Allmendinger & Shaw, 2000; Ferrill et al., 2012). In this study area, the basement faults are accommodating the stress from the ultraslow extension at the plate boundary. Therefore, we would expect episodic movement on the basement faults implying that the sedimentary faults would have also grown over a much longer period than in a faster spreading environment. We suggest that this has also had consequences for fluid migration within this system.

5.2. Fluid Migration Evolution

The fluid migration system on Svyatogor Ridge is unique in that it occurs in a sedimented mid-ocean ridge system where the basement rock is identified only ~500 ms TWT beneath the seafloor. Additionally, all the fluid flow features, such as the BSR and pockmarks, occur exclusively above the basement faults. Although it is not clear whether the system is still actively leaking fluid today, buried pockmarks occurring along certain stratigraphic horizons would indicate episodic fluid release events. In such large water depths, temperature and pressure changes due to sea-level fluctuations during glacial cycles are unlikely to have had a significant effect on the dynamics of a gas hydrate and associated fluid flow system here. However, it remains uncertain whether glacial related isostatic adjustments as modeled on the West Svalbard shelf (Wallmann et al., 2018) may have influenced fault activity and fluid migration on Svyatogor Ridge.

Johnson et al. (2015) proposed that the basement faults imaged on Svyatogor Ridge are acting as fluid migration pathways for fluids from the mid-ocean ridge system to reach the shallow subsurface. In this scenario, periods of fluid activity (migration and release from the seafloor) are most likely tectonically controlled. As noted previously, faulting events on BF1 and BF2 have occurred as recently as the time Unit S2 was deposited.

On the seafloor, pockmarks occur above both the chimney zone and above faults 50–100 m east of the chimney zone. Buried pockmarks, however, occur only within the chimney zone and not associated with

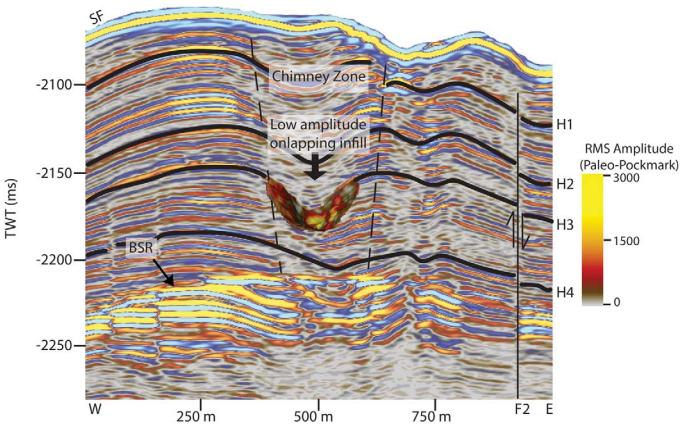

Figure 8. Paleo-pockmarks occur only within the Chimney zone, bordered by two sedimentary faults which are pervasive through the data, F1 and F2 (F2 annotated here). The paleo-pockmarks occur beneath the crest of the ridge, where the BSR is shallowest. One paleo-pockmark is highlighted in this figure, with the base of the paleo-pockmark displayed using RMS amplitude attribute to highlight that the paleo-pockmarks are circular-elliptical in shape and have a higher amplitude base than infill. Additionally, there is a higher amplitude at the base of the depression than the flanks, indicated by the RMS amplitude attribute. The infill is characterized by being onlapping against the base of the pockmark.

the faults to the east (Figures 8 and 9). This indicates that fluids bypassing the GHSZ have found an additional pathway over time; from releasing at paleo-seafloor(s) at the apex of the ridge indicated by paleo-pockmarks within the chimney zone to utilizing zones of weakness and fault planes, which culminates in pockmarks above faults. We interpret that this is a function of the time taken for sedimentary faults to develop. As shown in Figure 11, below the GHSZ fluid is able to utilize faults as migration pathways to the point of encountering the fold at the upper termination—the fold is acting as a structural seal. If the pore spaces of the sediment become overpressurized before another section of folded strata breaches into faults, fluid release to the seafloor will be characterized by "blow-out" type seal bypass systems (Cartwright et al., 2007) such as a chimney. As sedimentary faults propagate upward toward the seafloor they provide an additional seal bypass pathway (Figure 11). We have also identified small fracture networks, which are important in transporting fluid through the GHSZ. These fracture networks have randomly oriented strikes and therefore are not a consequence of the regional tectonic regime. We suggest that fracture networks are a consequence of hydraulic fracturing, occurring as fluids migrate through the subsurface. Small faults themselves have random strikes, but to the east of the free gas zone, these faults become integrated with sedimentary faults striking in compliance with the regional tectonic regime. Fracture networks appear to be restricted to a zone immediately above and within the free gas zone. We suggest that this is evidence for how fluid bypassed a seal created by hydrate clogging the pore space, a model consistent with Hornbach et al. (2004). We suggest that faults or planes of weakness were created in the past when the radial faulting formed that were then reactivated as the free gas zone became critically thick (Hornbach et al., 2004). In this scenario, planes of weakness across the seal need only be reactivated so that overpressure is released, and fluid can migrate upward without obstruction. We cannot determine from seismic data alone the type of brittle failure that is occurring to create these fractures (i.e., hydraulic extension fractures, extensional shear fractures, or meshes) (Sibson, 2003). However, we propose that in this case gas hydrate within the pore space of the sediment and the natural anticlinal structure of the ridge acts as an effective seal or cap rock. The fracture networks we identify here could be seismic evidence for the extent of the seal trapping free gas in this study location (Hornbach et al., 2004; Sibson, 2003).

Given that there are buried pockmarks found at ~30 ms TWT (~22 m) above the current BSR, and ~60 ms TWT (~45 m) above YP2–3 (Figures 9 and 11), gas migration into the free gas zone, gas hydrate formation, and migration to the (paleo-)seafloor has been ongoing during most of S1 deposition (Figures 2 and 11). Johnson et al. (2015) proposed that abiotic methane from serpentinization could be the origin of much of the gas here on Svyatogor Ridge. Our research suggests that the detachment faults here have indeed played a major role in driving fluid migration and expulsion in the subsurface and that methane may well have originated within these faults through serpentinization.

5.3. Consequence of Active Margin, Deep Ocean Setting on the Gas Hydrate and Fluid Flow System

The location of the Svyatogor Ridge on the flank of the Knipovich Ridge, atop detachment faults (which accommodate rifting), makes it a unique location for a gas hydrate and fluid flow system. In general the types of fluid flow systems normally identified on the flanks of spreading ridges are high temperature basalt hosted hydrothermal vent systems, generated by the increased heat flow provided by magmatic centers along axis (e.g., Guaymas Basin (Lizarralde et al., 2011)) or lower temperature peridotite hosted hydrothermal systems sustained by water-rock serpentinization reactions (e.g., Lost City Hydrothermal Field (Kelley et al., 2005)). In the case of the northern Knipovich Ridge, the ultraslow spreading regime, accommodated by observed detachment faults, implies it is a magma-limited environment, which would be inherently a lower temperature subseafloor regime, suitable for the development of the observed, stable gas hydrate system. There is documentation of magmatic instrusive bodies on the eastern flank of the Northern

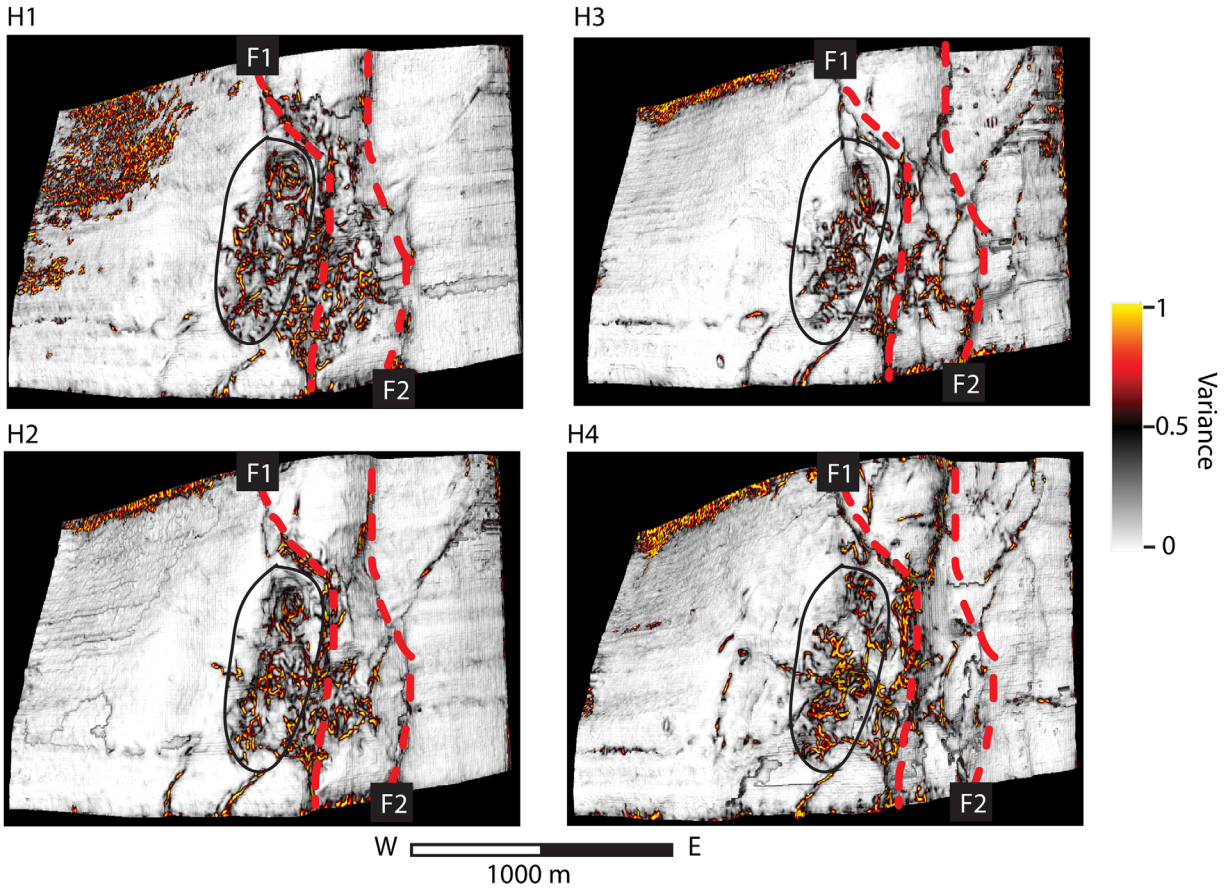

Figure 9. In variance attribute taken across horizons, the chimney zone (black oval) is characterized by being highly variant, but chaotic. The first two pervasive sedimentary faults (F1 and F2, red dotted lines) are clear in all four variance maps, and border the chimney zone to the east. Locations of horizons shown in Figures 2 and 8.

Knipovich Ridge (Ritzmann et al., 2004), which would have presumably formed in conjunction with rifting on either the Molloy Ridge or the Knipovich Ridge, in a mixed mode scenario of detachment fault and magmatic spreading in the past; however, other studies have not found evidence for magmatic instrusive bodies associated with the northern section of the Knipovich Ridge (i.e., Amundsen et al., 2011; Crane et al., 2001). Partial serpentinization of the crust at this location is supported by Ritzmann et al. (2004) who observe crustal velocities of ~7.6 km/s south of the Molloy Transform Fault. Hydrothermal system studies further south along the Knipovich Ridge also suggest that there is some methane flux from serpentinization along with other hydrothermally generated fluids (Cannat et al., 2010). That a fluid flow system exists on a spreading ridge is not unique in itself due to the abundance of hydrothermal systems present on mid-ocean ridges, but the lack of significant heat flow and therefore, potential for a stable gas hydrate stability zone, is an interesting case for Svyatogor Ridge, as gas hydrate systems are normally identified on passive continental margins, far from spreading ridges. Most of the world's oceans deeper than approximately 300 mbsl have potential for gas hydrate stability (Kvenvolden, 1993). However, a distal setting is commonly excluded from global gas hydrate concentration models due to a lack of organic matter deposition (Klauda & Sandler, 2005). A possible exception to this is of course in the case where the Continental-Oceanic crust boundary is proximal to a sediment source and has been active for a long period of time, for example, in the Gulf of Mexico or in the Fram Strait at Vestnesa Ridge. On the Svyatogor Ridge, however, asymmetric, ultraslow spreading of the Knipovich Ridge means that the Svyatogor Ridge has, since the underlying crust formed, been in proximity to the West Svalbard Margin and West Spitsbergen Current, allowing sedimentation at the northern extent of the Knipovich Ridge flanks (Eiken & Hinz, 1993; Johnson et al., 2015) and therefore providing suitable reservoir material for fluids generated by crustal processes.

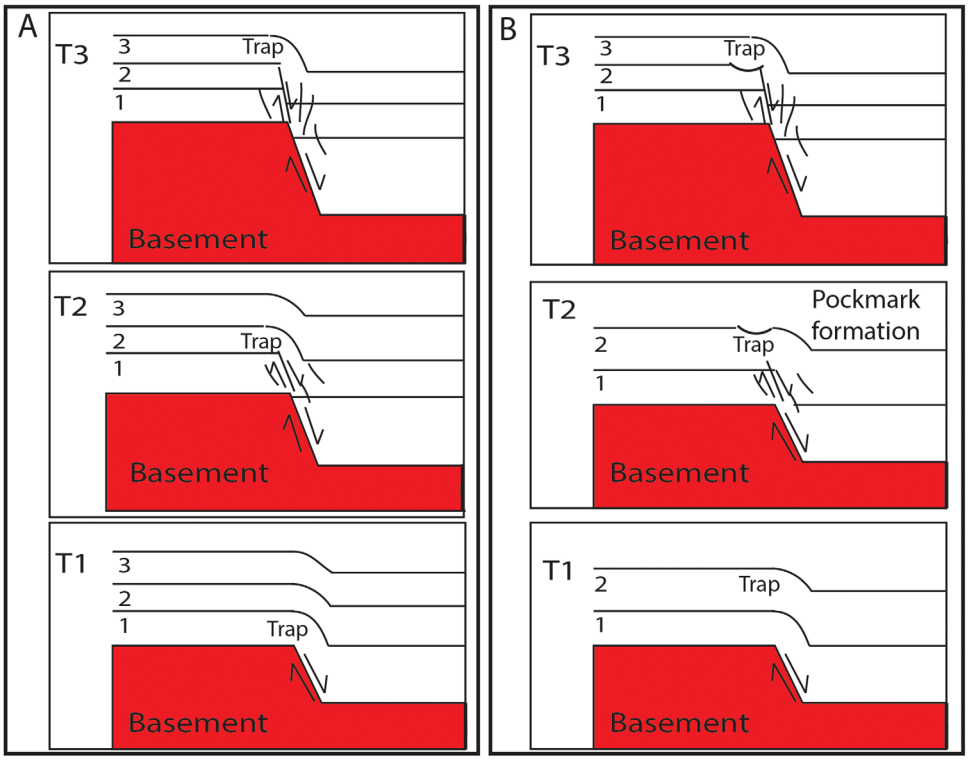

Figure 10. (a) Conceptual diagram of fault growth where a mechanically stronger basement, covered by a mechanically weaker strata, faults and causes folds to develop, and with continued movement on the basement fault these folds breach into faults. In this simple scenario, fluid () can utilize the faulted sections to migrate but may become trapped (labeled "trap") by the unfaulted strata (after Hardy & McClay, 1999). (b) When this process occurs close to the seafloor, fluid seepage across the seafloor results in pockmark formation. With continued syn-deformation sedimentation, pockmarks get buried and the process continues.

The occurrence of a gas hydrate system on the flank of an actively spreading margin presents an interesting case because active margin hydrate systems are better studied and more prolific on subduction margins, for example, the Hikurangi (Barnes et al., 2010; Crutchley et al., 2010; Faure et al., 2006; Pecher et al., 2005) and Cascadia margins (Bohrmann et al., 1998; Pohlman et al., 2009; Riedel & Collett, 2005; Suess et al., 1999). In a compressional tectonic system, we expect to identify particular structural fabrics related to the regional tectonic regime. However, these structural fabrics will differ in an extensional regime, and while we can compare a gas hydrate system in an extensional setting to, for example, a hydrothermal system in terms of fluid flow pathway development, the Svyatogor Ridge setting may be confounded by two additional factors: (1) the location proximal to a strike-slip tectonic setting could be influencing the tectonic setting and (2) it is difficult to determine what effect, if any, an ultraslow spreading regime has on the coupling between fluid migration pathway development, seepage and tectonic development. In this initial investigation of Svyatogor Ridge, we have not been able to determine with precision if the Molloy Transform Fault has an influence on the structural fabric and therefore fluid flow regime; however, we have posited that the ultraslow nature of the Knipovich Ridge might have played a role in the timing of fluid release on the Svyatogor Ridge. In contrast to the tectonic setting on Vestnesa Ridge, which is a contourite drift developed close to the mid-ocean ridge but on a passive margin slope, (Bünz et al., 2012; Plaza-Faverola et al., 2015; Vanneste et al., 2005), Svyatogor Ridge appears to be unique in that sedimentary sequences, the gas hydrate system, and the tectonic setting are developing in unison, particularly reliant on the tectonic setting to form as they have.

5.4. A Note on Gas Origin

Shallow penetrating gravity cores collected on Svyatogor Ridge during CAGE expeditions have yet to recover enough gas for isotopic analysis. As there are no other gas samples from the Svyatogor Ridge available to the authors, we note from the 3-D seismic survey that (1) faults appear to be controlling where and

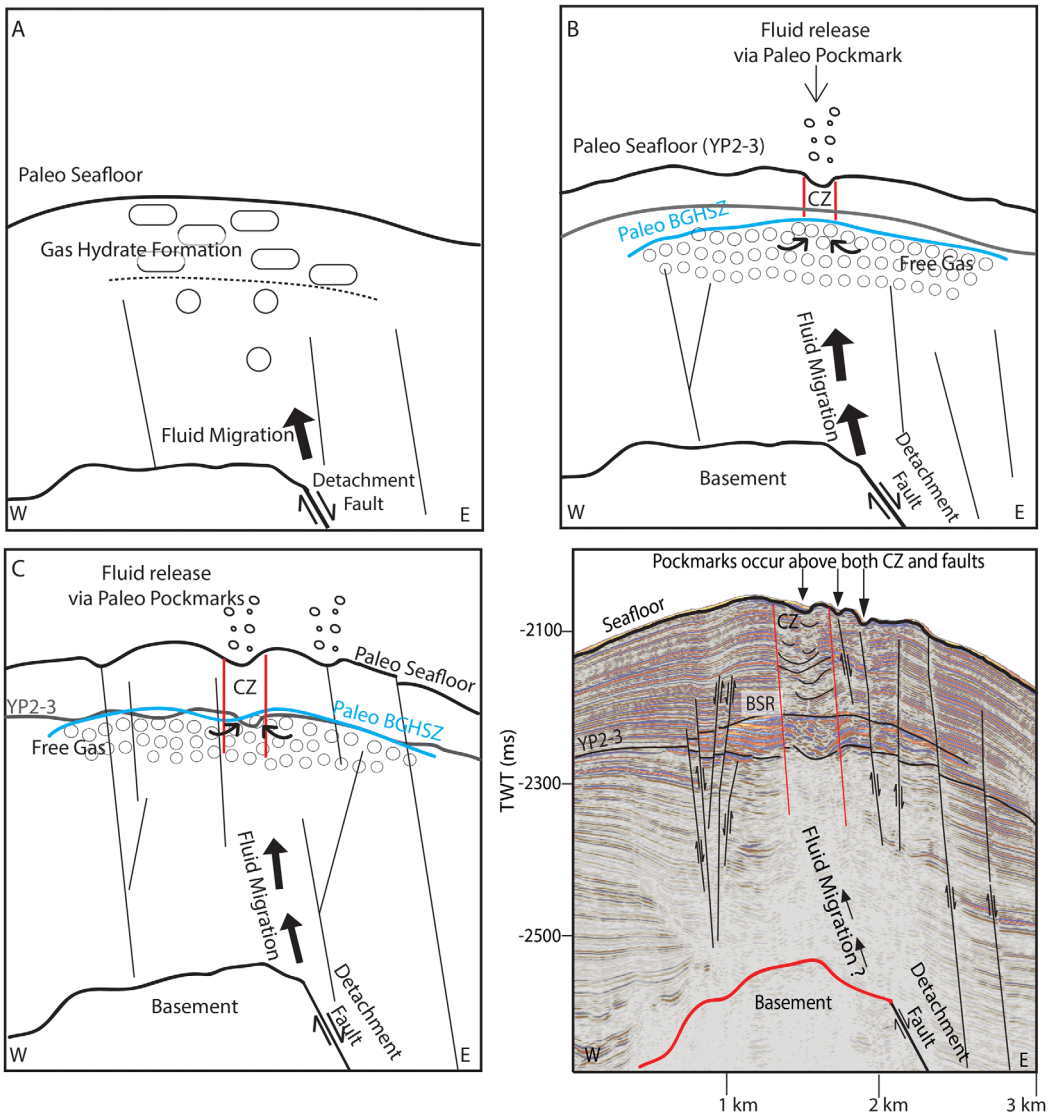

Figure 11. (a) During initial activation of the detachment fault, faults in the sedimentary strata had not propagated far through the sedimentary column so they were not fluid migration pathways to the seafloor. However, gas hydrate can develop as can a free gas zone. (b) With prolonged fluid migration into the system, fluids in the FGZ can become over-pressurized and force the chimney zone to form (c). As additional material deposited, the BGHSZ is able to migrate upward, and sedimentary faults propagated further due to further movement on detachment fault. This means that fluid migrating to the seafloor is able to use faults as fluid migration pathways to the seafloor. (d) Today, it is not clear whether the detachment faults are supplying fluid to Svyatogor Ridge; however, the evidence of past fluid migration and release is preserved.

how the gas hydrate system has formed and that (2) the detachment faults are the major linking factor to all the processes occurring on the Svyatogor Ridge (sedimentary fault development, fluid flow pathway development, and ridge topography). With regards to thermogenic gas production, we posit that there has been no thermogenic methane produced within the sediments on the Svyatogor Ridge itself as the criterion for generation (normally depths greater than 1,000 m below seafloor (Floodgate & Judd, 1992)) is not met. We cannot rule out that there is gas migrating from another source, for example, across the Molloy Transform Fault (Smith et al., 2014) or from Hovgård Ridge (Knies et al., 2018), which has also been shown to have some source rock present (Knies & Mann, 2002). We do note, however, that methane is generated in serpentinization reactions (Etiope & Sherwood Lollar, 2013) and that Cannat et al. (2010) and Proskurowski et al. (2008) show methane production from serpentinization is produced in slow to ultraslow spreading ridge settings. Additionally, Ritzmann et al. (2004) shows that there is potential for partially serpentinized

crust beneath Svyatogor Ridge. Given that the detachment faults are key for the dynamics of this gas hydrate system, we would not rule out some contribution from serpentinization produced methane. Active methane production via serpentinization beneath the study location today may be unlikely, however, as the detachment faults now are approaching the end, or are at the end, of their typical duration of activity (1–3 My), sedimentation above the oceanic crust restricts seawater peridotite interaction, and continued spreading and offset along the MTF has nearly removed Svyatogor Ridge sediments from the serpentinization driven abiotic methane window suggested by Johnson et al. (2015). Thus, any abiotic methane present within the gas hydrate system here today, must have formed while the detachment faults were active, Svyatogor Ridge was within the abiotic methane production window, and there was sufficient sedimentation to trap the gases. In this scenario, methane generated through serpentinization may be preserved in early developing gas hydrate systems, like Svyatogor Ridge, but with continued development, the influence of crustal sources of fluids and gases may be minimized. Given the history here, we associate the modern fluid flow system in this study area as a sediment hosted gas hydrate system that developed over the last ~3 million years.

6. Conclusion

The Svyatogor Ridge has developed on the North Western flank of the Knipovich Ridge in an active margin setting. The majority of sedimentation on the Svyatogor Ridge has been interpreted to deposit during the YP-2 and YP-3 sedimentation regimes, while the Svyatogor Ridge was still close to the spreading center and an active sediment supply. The tectonic environment here has greatly controlled all aspects of development in this setting, from sedimentary evolution to fluid flow system evolution. Sedimentary faults in the 3-D seismic data are directly linked to the movement on spreading related detachment faults and the seismic stratigraphy is largely based on changes of reflection patterns linked to phases of faulting on detachment faults. The gas hydrate system on the Svyatogor Ridge is located on the flank of the Knipovich ridge axis—in a natural trapping structure along the crest of the Svyatogor Ridge. Seepage from this system to the water column has been episodic in nature, occurring at four distinct intervals throughout the last ~2.7 Ma. Tectonism appears to be the major driver of fluid flow on Svyatogor Ridge, with movement on detachment faults shown to be impacting both the fluid flow into the gas hydrate and free gas zones, and release of at the (paleo-)seafloor.

Subaqueous gas hydrate reservoirs are generally found in settings with thick sedimentary sequences: on passive continental margins, contourite deposits, or active (subducting) continental margins. Svyatogor Ridge, however, is a sediment-limited, deep water drift located on an actively spreading plate boundary. Worldwide, this setting type is generally dominated by hydrothermal fluid systems sustained by seawater circulation in basalt or peridotite dominated crust. Due to the amagmatic nature of the northern Knipovich Ridge, there is no significant heat source for a magmatically heated hydrothermal system. Hydrothermal systems further south along the Knipovich Ridge have been shown to have methane as a fluid constituent, due to serpentinization reactions, and on the Svyatogor Ridge studies have shown that the acoustic velocity of basement material give a likelihood of serpentinitized mantle beneath the Svyatogor Ridge. Therefore, we conclude that the Svyatogor Ridge has developed a gas hydrate system in this ultraslow, amagmatic spreading setting largely due to the presence of detachment faults, which accommodate seafloor spreading and deformation of the overlying sediment column, enable seawater rock reactions to drive serpentinization, and serve as pathways for crustal fluid and gas migration to the overlying sediments.

Acknowledgments
This work was supported by the Research Council of Norway through its Centres of Excellence funding scheme, project 223259. We acknowledge the crew and scientific party aboard the R.V. Helmer Hanssen during CAGE expeditions 14-1, 14-2, and 15-6. We thank the reviewers for their insightful comments and suggestions for improvement. We also acknowledge Schlumberger for providing interpretational software. Seismic data can be accessed at UiT Open Research Data Repository.

References

Allmendinger, R. W., & Shaw, J. H. (2000). Estimation of fault propagation distance from fold shape: Implications for earthquake hazard assessment. *Geology*, *28*(12), 1099–1102. https://doi.org/10.1130/0091-7613(2000)28<1099:EOFPDF>2.0.CO;2

Amundsen, I. M. H., Blinova, M., Hjelstuen, B. O., Mjelde, R., & Haflidason, H. (2011). The Cenozoic western Svalbard margin: Sediment geometry and sedimentary processes in an area of ultraslow oceanic spreading. *Marine Geophysical Research*, *32*(4), 441–453. https://doi.org/10.1007/s11001-011-9127-z

Anderson, A. L., & Hampton, L. D. (1980). Acoustics of gas-bearing sediments I. Background. *The Journal of the Acoustical Society of America*, *67*(6), 1865–1889. https://doi.org/10.1121/1.384453

Barnes, P. M., Lamarche, G., Bialas, J., Henrys, S., Pecher, I., Netzeband, G. L., et al. (2010). Tectonic and geological framework for gas hydrates and cold seeps on the Hikurangi subduction margin, New Zealand. *Marine Geology*, *272*(1–4), 26–48.

Beszczynska-Möller, A., Fahrbach, E., Schauer, U., & Hansen, E. (2012). Variability in Atlantic water temperature and transport at the entrance to the Arctic Ocean, 1997–2010. *ICES Journal of Marine Science: Journal Du Conseil*, *69*(5), 852–863. https://doi.org/10.1093/icesjms/fss056

Bodego, A., & Agirrezabala, L. M. (2013). Syn-depositional thin-and thick-skinned extensional tectonics in the mid-Cretaceous Lasarte subbasin, western Pyrenees. *Basin Research*, *25*(5), 594–612. https://doi.org/10.1111/bre.12017
Bohrmann, G., Greinert, J., Suess, E., & Torres, M. (1998). Authigenic carbonates from the Cascadia subduction zone and their relation to gas hydrate stability. *Geology*, *26*(7), 647–650.
Bünz, S., Polyanov, S., Vadakkepuliyambatta, S., Consolaro, C., & Mienert, J. (2012). Active gas venting through hydrate-bearing sediments on the Vestnesa Ridge, offshore W-Svalbard. *Marine Geology*, *332–334*, 189–197. https://doi.org/10.1016/j.margeo.2012.09.012
Cann, J., Blackman, D., Smith, D., McAllister, E., Janssen, B., Mello, S., et al. (1997). Corrugated slip surfaces formed at ridge-transform intersections on the Mid-Atlantic Ridge. *Nature*, *385*(6614), 329. https://doi.org/10.1038/385329a0
Cannat, M., Fontaine, F., & Escartin, J. (2010). Serpentinization and associated hydrogen and methane fluxes at slow spreading ridges. In Rona, P. A., Devey, C. W., Dyment, J., & Murton, B. J. (Eds.), *Diversity of hydrothermal systems on slow spreading ocean ridges* (pp. 241–264). Washington, DC: American Geophysical Union.
Cartwright, J., Huuse, M., & Aplin, A. (2007). Seal bypass systems. *AAPG Bulletin*, *91*(8), 1141–1166. https://doi.org/10.1306/04090705181
Cartwright, J., & Santamarina, C. (2015). Seismic characteristics of fluid escape pipes in sedimentary basins: Implications for pipe genesis. *Marine and Petroleum Geology*, *65*, 126–140. https://doi.org/10.1016/j.marpetgeo.2015.03.023
Corfield, S., & Sharp, I. (2000). Structural style and stratigraphic architecture of fault propagation folding in extensional settings: A seismic example from the Smørbukk area, Halten Terrace, Mid-Norway. *Basin Research*, *12*(3–4), 329–341. https://doi.org/10.1111/j.1365-2117.2000.00133.x
Crane, K., Doss, H., Vogt, P., Sundvor, E., Cherkashov, G., Poroshina, I., et al. (2001). The role of the Spitsbergen shear zone in determining morphology, segmentation and evolution of the Knipovich Ridge. *Marine Geophysical Researches*, *22*(3), 153–205. https://doi.org/10.1029/91JB01231
Crutchley, G. J., Pecher, I. A., Gorman, A. R., Henrys, S. A., & Greinert, J. (2010). Seismic imaging of gas conduits beneath seafloor seep sites in a shallow marine gas hydrate province, Hikurangi Margin, New Zealand. *Marine Geology*, *272*(1–4), 114–126.
Dick, H. J., Lin, J., & Schouten, H. (2003). An ultraslow-spreading class of ocean ridge. *Nature*, *426*(6965), 405–412. https://doi.org/10.1038/nature02128
Eagles, G., Pérez-Díaz, L., & Scarselli, N. (2015). Getting over continent ocean boundaries. *Earth-Science Reviews*, *151*, 244–265.
Ehlers, B.-M., & Jokat, W. (2009). Subsidence and crustal roughness of ultra-slow spreading ridges in the northern North Atlantic and the Arctic Ocean. *Geophysical Journal International*, *177*(2), 451–462. https://doi.org/10.1111/j.1365-246X.2009.04078.x
Eiken, O., & Hinz, K. (1993). Contourites in the Fram Strait. *Sedimentary Geology*, *82*(1–4), 15–32. https://doi.org/10.1016/0037-0738(93)90110-Q
Engen, Ø., Faleide, J. I., & Dyreng, T. K. (2008). Opening of the Fram Strait gateway: A review of plate tectonic constraints. *Tectonophysics*, *450*(1–4), 51–69. https://doi.org/10.1016/j.tecto.2008.01.002
Escartin, J., Smith, D. K., Cann, J., Schouten, H., Langmuir, C. H., & Escrig, S. (2008). Central role of detachment faults in accretion of slow-spreading oceanic lithosphere. *Nature*, *455*(7214), 790–794. https://doi.org/10.1038/nature07333
Etiope, G., & Sherwood Lollar, B. (2013). Abiotic methane on Earth. *Reviews of Geophysics*, *51*, 276–299. https://doi.org/10.1002/rog.20011
Faure, K., Greinert, J., Pecher, I. A., Graham, I. J., Massoth, G. J., De Ronde, C. E., et al. (2006). Methane seepage and its relation to slumping and gas hydrate at the Hikurangi margin, New Zealand. *New Zealand Journal of Geology and Geophysics*, *49*(4), 503–516.
Faugeres, J.-C., Stow, D. A., Imbert, P. & Viana, A. (1999). Seismic features diagnostic of contourite drifts. *Marine Geology*, *162*, 1–38. https://doi.org/10.1016/S0025-3227(99)00068-7
Ferrill, D. A., Morris, A. P., & McGinnis, R. N. (2012). Extensional fault-propagation folding in mechanically layered rocks: The case against the frictional drag mechanism. *Tectonophysics*, *576–577*, 78–85. https://doi.org/10.1016/j.tecto.2012.05.023
Floodgate, G., & Judd, A. (1992). The origins of shallow gas. *Continental Shelf Research*, *12*(10), 1145–1156.
Geissler, W. H., Jokat, W., & Brekke, H. (2011). The Yermak Plateau in the Arctic Ocean in the light of reflection seismic data-implication for its tectonic and sedimentary evolution. *Geophysical Journal International*, *187*(3), 1334–1362. https://doi.org/10.1111/j.1365-246X.2011.05197.x
Hansen, J., Cartwright, J., Huuse, M., & Clausen, O. R. (2005). 3D seismic expression of fluid migration and mud remobilization on the Gjallar Ridge, offshore mid-Norway. *Basin Research*, *17*(1), 123–139. https://doi.org/10.1111/j.1365-2117.2005.00257.x
Hardy, S., & McClay, K. (1999). Kinematic modelling of extensional fault-propagation folding. *Journal of Structural Geology*, *21*(7), 695–702. https://doi.org/10.1016/S0191-8141(99)00072-3
Hartwig, A., Anka, Z., & di Primio, R. (2012). Evidence of a widespread paleo-pockmarked field in the Orange Basin: An indication of an early Eocene massive fluid escape event offshore South Africa. *Marine Geology*, *332–334*, 222–234.
Holbrook, W. S., Hoskins, H., Wood, W. T., Stephen, R. A., & Lizarralde, D. (1996). Methane hydrate and free gas on the Blake Ridge from vertical seismic profiling. *Science*, *273*(5283), 1840. https://doi.org/10.1126/science.273.5283.1840
Hornbach, M. J., Saffer, D. M., & Steven Holbrook, W. (2004). Critically pressured free-gas reservoirs below gas-hydrate provinces. *Nature*, *427*(6970), 142–144. https://doi.org/10.1038/nature02172
Howe, J. A., Shimmield, T. M., Harland, R., & Eyles, N. (2008). Late Quaternary contourites and glaciomarine sedimentation in the Fram Strait. *Sedimentology*, *55*, 179–200. https://doi.org/10.1111/j.1365-3091.2007.00897.x
Hustoft, S., Bünz, S., Mienert, J., & Chand, S. (2009). Gas hydrate reservoir and active methane-venting province in sediments on $<$20 Ma young oceanic crust in the Fram Strait, offshore NW-Svalbard. *Earth and Planetary Science Letters*, *284*(1–2), 12–24. https://doi.org/10.1016/j.epsl.2009.03.038
Jackson, C., Gawthorpe, R., & Sharp, I. (2006). Style and sequence of deformation during extensional fault-propagation folding: Examples from the Hammam Faraun and El-Qaa fault blocks, Suez Rift, Egypt. *Journal of Structural Geology*, *28*(3), 519–535. https://doi.org/10.1016/j.jsg.2005.11.009
Johnson, J. E., Mienert, J., Plaza-Faverola, A., Vadakkepuliyambatta, S., Knies, J., Bünz, S., et al. (2015). Abiotic methane from ultraslow-spreading ridges can charge Arctic gas hydrates. *Geology*, *43*(5), 371–374. https://doi.org/10.1130/G36440.1
Kelley, D. S., Karson, J. A., Früh-Green, G. L., Yoerger, D. R., Shank, T. M., Butterfield, D. A., et al. (2005). A serpentinite-hosted ecosystem: The Lost City hydrothermal field. *Science*, *307*(5714), 1428–1434.
Klauda, J. B., & Sandler, S. I. (2005). Global distribution of methane hydrate in ocean sediment. *Energy & Fuels*, *19*(2), 459–470.
Knies, J., Daszinnies, M., Plaza-Faverola, A., Chand, S., Sylta, Ø., Bünz, S., et al. (2018). Modelling persistent methane seepage offshore western Svalbard since early Pleistocene. *Marine and Petroleum Geology*, *91*, 800–811. https://doi.org/10.1016/j.marpetgeo.2018.01.020
Knies, J., & Mann, U. (2002). Depositional environment and source rock potential of Miocene strata from the central Fram Strait: Introduction of a new computing tool for simulating organic facies variations. *Marine and Petroleum Geology*, *19*(7), 811–828.
Kvenvolden, K. A. (1993). Gas hydrates-geological perspective and global change. *Review of Geophysics*, *31*(2), 173–187. https://doi.org/10.1029/93RG00268

Lizarralde, D., Soule, S. A., Seewald, J. S., & Proskurowski, G. (2011). Carbon release by off-axis magmatism in a young sedimented spreading centre. *Nature Geoscience*, *4*(1), 50–54.
Lundin, E., & Doré, A. (2002). Mid-Cenozoic post-breakup deformation in the 'passive' margins bordering the Norwegian-Greenland Sea. *Marine and Petroleum Geology*, *19*(1), 79–93. https://doi.org/10.1016/S0264-8172(01)00046-0
Løseth, H., Gading, M., & Wensaas, L. (2009). Hydrocarbon leakage interpreted on seismic data. *Marine and Petroleum Geology*, *26*(7), 1304–1319. https://doi.org/10.1016/j.marpetgeo.2008.09.008
Mattingsdal, R., Knies, J., Andreassen, K., Fabian, K., Husum, K., Grøsfjeld, K., et al. (2014). A new 6 Myr stratigraphic framework for the Atlantic-Arctic Gateway. *Quaternary Science Reviews*, *92*, 170–178. https://doi.org/10.1016/j.quascirev.2013.08.022
Michael, P., Langmuir, C., Dick, H., Snow, J., Goldstein, S., Graham, D., et al. (2003). Magmatic and amagmatic seafloor generation at the ultraslow-spreading Gakkel ridge, Arctic Ocean. *Nature*, *423*(6943), 956–961. https://doi.org/10.1038/nature01704
Müller, P. J., & Suess, E. (1979). Productivity, sedimentation rate, and sedimentary organic matter in the oceans—I. Organic carbon preservation. *Deep-Sea Research Part A*, *26*(12), 1347–1362.
Okino, K., Curewitz, D., Asada, M., Tamaki, K., Vogt, P., & Crane, K. (2002). Preliminary analysis of the Knipovich Ridge segmentation: Influence of focused magmatism and ridge obliquity on an ultraslow spreading system. *Earth and Planetary Science Letters*, *202*(2), 275–288. https://doi.org/10.1016/S0012-821X(02)00790-2
Paull, C. K., Ussle, W., & Borowski, W. S. (1994). Sources of biogenic methane to form marine gas hydrates in situ production or upward migration? *Annals of the New York Academy of Sciences*, *715*(1), 392–409.
Pecher, I., Henrys, S., Ellis, S., Chiswell, S., & Kukowski, N. (2005). Erosion of the seafloor at the top of the gas hydrate stability zone on the Hikurangi Margin, New Zealand. *Geophysical Research Letters*, *32*, L24603. https://doi.org/10.1029/2005GL024687
Peel, F. J. (2014). The engines of gravity-driven movement on passive margins: Quantifying the relative contribution of spreading vs. gravity sliding mechanisms. *Tectonophysics*, *633*, 126–142. https://doi.org/10.1016/j.tecto.2014.06.023
Peive, A., & Chamov, N. (2008). Basic tectonic features of the Knipovich Ridge (North Atlantic) and its neotectonic evolution. *Geotectonics*, *42*(1), 31–47. https://doi.org/10.1134/S0016852108010044
Planke, S., Erikson, F. N., Berndt, C., Mienert, J., & Masson, D. (2009). P-Cable high-resolution seismic. *Oceanography*, *22*(1), 85. https://doi.org/10.5670/oceanog.2009.09
Plaza-Faverola, A., Bünz, S., Johnson, J. E., Chand, S., Knies, J., Mienert, J., et al. (2015). Role of tectonic stress in seepage evolution along the gas hydrate-charged Vestnesa Ridge, Fram Strait. *Geophysical Research Letters*, *42*, 733–742. https://doi.org/10.1002/2014GL062474
Pohlman, J., Kaneko, M., Heuer, V., Coffin, R., & Whiticar, M. (2009). Methane sources and production in the northern Cascadia margin gas hydrate system. *Earth and Planetary Science Letters*, *287*(3–4), 504–512.
Proskurowski, G., Lilley, M. D., Seewald, J. S., Fru h-Green, G. L., Olson, E. J., Lupton, J. E., et al. (2008). Abiogenic hydrocarbon production at Lost City hydrothermal field. *Science*, *319*(5863), 604–607.
Rajan, A., Mienert, J., Bünz, S., & Chand, S. (2012). Potential serpentinization, degassing, and gas hydrate formation at a young (<20 Ma) sedimented ocean crust of the Arctic Ocean ridge system. *Journal of Geophysical Research*, *117*, B03102. https://doi.org/10.1029/2011JB008537
Rebesco, M., Wåhlin, A., Laberg, J. S., Schauer, U., Beszczynska-Möller, A., Lucchi, R. G., et al. (2013). Quaternary contourite drifts of the Western Spitsbergen margin. *Deep-Sea Research Part I*, *79*, 156–168. https://doi.org/10.1016/j.dsr.2013.05.013
Riedel, M., & Collett, T. (2005). *Cascadia margin gas hydrates* (IODP Preliminary Rep. 311). College Station, TX: Ocean Drilling Program.
Ritzmann, O., Jokat, W., Czuba, W., Guterch, A., Mjelde, R., & Nishimura, Y. (2004). A deep seismic transect from Hovgård Ridge to northwestern Svalbard across the continental-ocean transition: A sheared margin study. *Geophysical Journal International*, *157*(2), 683–702. https://doi.org/10.1111/j.1365-246X.2004.02204.x
Shipley, T. H., Houston, M. H., Buffler, R. T., Shaub, F. J., McMillen, K. J., Ladd, J. W., et al. (1979). Seismic evidence for widespread possible gas hydrate horizons on continental slopes and rises. *AAPG Bulletin*, *63*(12), 2204–2213. https://doi.org/10.1306/2f91890a-16ce-11d7-8645000102c1865d
Sibson, R. H. (2003). Brittle-failure controls on maximum sustainable overpressure in different tectonic regimes. *AAPG Bulletin*, *87*(6), 901–908. https://doi.org/10.1306/01290300181
Sloan, E. D. (1998). Gas hydrates: Review of physical/chemical properties. *Energy & Fuels*, *12*(2), 191–196. https://doi.org/10.1021/ef970164+
Smith, A. J., Mienert, J., Bünz, S., & Greinert, J. (2014). Thermogenic methane injection via bubble transport into the upper Arctic Ocean from the hydrate-charged Vestnesa Ridge, Svalbard. *Geochemistry, Geophysics, Geosystems*, *15*, 1945–1959. https://doi.org/10.1002/2013GC005179
Snow, J., Hellebrand, E., Jokat, W., & Mühe, R. (2001). Magmatic and hydrothermal activity in Lena Trough, Arctic Ocean. *EOS, Transactions American Geophysical Union*, *82*(17), 193–198. https://doi.org/10.1029/01EO00101
Suess, E., Torres, M., Bohrmann, G., Collier, R., Greinert, J., Linke, P., et al. (1999). Gas hydrate destabilization: Enhanced dewatering, benthic material turnover and large methane plumes at the Cascadia convergent margin. *Earth and Planetary Science Letters*, *170*(1–2), 1–15.
Talwani, M., & Eldholm, O. (1977). Evolution of the Norwegian-Greenland sea. *Geological Society of America Bulletin*, *88*(7), 969–999. https://doi.org/10.1130/0016-7606(1977)88<969:EOTNS>2.0.CO;2
Tucholke, B. E., Lin, J., & Kleinrock, M. C. (1998). Megamullions and mullion structure defining oceanic metamorphic core complexes on the Mid-Atlantic Ridge. *Journal of Geophysical Research*, *103*(B5), 9857–9866. https://doi.org/10.1029/98JB00167
Tvedt, A. B., Rotevatn, A., Jackson, C. A.-L., Fossen, H., & Gawthorpe, R. L. (2013). Growth of normal faults in multilayer sequences: A 3D seismic case study from the Egersund Basin, Norwegian North Sea. *Journal of Structural Geology*, *55*, 1–20. https://doi.org/10.1016/j.jsg.2013.08.002
Vanneste, M., Guidard, S., & Mienert, J. (2005). Bottom-simulating reflections and geothermal gradients across the western Svalbard margin. *Terra Nova*, *17*(6), 510–516.
Vogt, P., Feden, R., Eldholm, O., & Sundvor, E. (1978). The ocean crust west and north of the Svalbard Archipelago: Synthesis and review of new results. *Polarforschung*, *48*(1/2), 1–19. https://doi.org/10.2312/polarforschung.48.1-2.1
Wallmann, K., Riedel, M., Hong, W. L., Patton, H., Hubbard, A., Pape, T., et al. (2018). Gas hydrate dissociation off Svalbard induced by isostatic rebound rather than global warming. *Nature Communications*, *9*, 83. https://doi.org/10.1038/s41467-017-02550-9